STEM CELLS AND DEVELOPMENT
Volume 31, Numbers 23–24, 2022

DOI: 10.1089/scd.2022.0053

Overexpression of NDST1 Attenuates Fibrotic Response in Murine Adipose-Derived Stem Cells

Takayoshi Otsuka,[1,2] Ho-Man Kan,[1,2] Timothy D. Mason,[1] Lakshmi S. Nair,[1–5] and Cato T. Laurencin[1–6]

Adipose-derived stem cells (ADSCs) hold tremendous potential for treating diseases and repairing damaged tissues. Heparan sulfate (HS) plays various roles in cellular signaling mechanisms. The importance of HS in stem cell function has been reported and well documented. However, there has been little progress in using HS for therapeutic purposes. We focused on one of the sulfotransferases, NDST1, which influences overall HS chain extent and sulfation pattern, with the expectation to enhance stem cell function by increasing the N-sulfation level. We herein performed transfections of a green fluorescent protein-vector control and NDST1-vector into mouse ADSCs to evaluate stem cell functions. Overexpression of NDST1 suppressed the osteogenic differentiation of ADSCs. There was no pronounced effect observed on the stemness, inflammatory gene expression, nor any noticeable effect in adipogenic and chondrogenic differentiation. Under the tumor necrosis factor-alpha stimulation, NDST1 overexpression induced several chemokine productions that attract neutrophils and macrophages. Finally, we identified an antifibrotic response in ADSCs overexpressing NDST1. This study provides a foundation for the evaluation of HS-related effects in ADSCs undergoing ex vivo gene manipulation.

Keywords: adipose-derived stem cells (ADSCs), nonviral gene delivery, nucleofection, heparan sulfate, NDST1, fibrosis

Introduction

In recent years, adipose-derived stem cells (ADSCs), a type of mesenchymal stromal cells, have been attracting interest in tissue regeneration [1,2]. In addition to the potential for self-renewal and multidirectional differentiation, paracrine factors secreted from ADSCs are mainly responsible for their therapeutic effect [3,4]. One of the notable features of ADSCs is their immunomodulatory effect, which includes suppression of B and T cell proliferation, induction of regulatory T cells, inhibition of NK cell function, and inhibition of dendritic cell maturation [5,6]. ADSCs have been reported to promote the polarization of the proinflammatory M1 macrophages to the anti-inflammatory M2 macrophages [7,8]. ADSCs have been shown to attenuate fibrosis through modulation of macrophage function [9–11]. These advantages ultimately drive the development of innovative strategies using ADSCs for tissue regeneration.

Heparan sulfate (HS) is a linear polysaccharide chain of repeating disaccharides of N-acetyl-glucosamine and uronic acid (glucuronic acid or iduronic acid) [12]. HS glycosaminoglycans (GAGs) attach to its core protein, heparan sulfate proteoglycans (HSPGs), which are enriched on the cell surface and extracellular matrix (ECM). The GAG chain length and degree of sulfation are highly heterogeneous and play critical roles in cellular signaling mechanisms by binding growth factors [13,14]. The diverse roles of HS have been reported such as mediators of stem cell function [15,16], fate commitment [17–19], inflammation [20,21], and regeneration [22,23]. Therefore, understanding

[1]Connecticut Convergence Institute for Translation in Regenerative Engineering, University of Connecticut Health, Farmington, Connecticut, USA.
[2]Raymond and Beverly Sackler Center for Biomedical, Biological, Physical and Engineering Sciences, University of Connecticut Health, Farmington, Connecticut, USA.
[3]Department of Orthopaedic Surgery, University of Connecticut Health, Farmington, Connecticut, USA.
Departments of [4]Biomedical Engineering, [5]Materials Science and Engineering, and [6]Chemical and Biomolecular Engineering, University of Connecticut, Storrs, Connecticut, USA.

and exploiting the multifaceted functions of HS is one of the key components of stem cell-based therapy.

HS function, especially the binding affinity to numerous molecules, depends on the sulfation patterns of the HS chain, which is regulated by various enzymes such as N-deacetylase-N-sulfotransferases (*NDSTs*), C5 epimerases (*HsGlce*), O-sulfotransferases (*Hs2st*, *Hs6sts*, and *Hs3sts*), and HS 6-O-endosulfatases (*sulf1/2*) [12]. Among them, NDSTs initiate modification reactions that have a key role in designing the extent and pattern of sulfation of the overall HS chain. The lack of NDST1 in Chinese hamster ovary cells led to an undersulfated and less spatial distribution that affects HS function [24]. On the contrary, NDST1 (or NDST2) overexpression increased the level of N-sulfation in human kidney 293 cells [25]. The essential role of N-sulfation in early differentiation has been revealed through the NDST1/2 knockout embryonic stem cells (ESCs) [26]. However, the effect of NDST1 on adult stem cell behavior remains largely unknown.

HS also plays a key role during the wound healing process via regulating inflammatory response, signaling pathway, and ECM remodeling [27]. The deletion of NDST1 in endothelial cells has been reported to reduce leukocyte recruitment and neutrophil infiltration [28]. Delayed wound healing has been found in HSPG-deficient mice such as perlecan or syndecan-4 deficient mice [29,30]. The degradation of HS by heparinase showed accelerated cutaneous wound healing in mouse and rat models [31]. Moreover, the upregulation of O-sulfation has been found in renal and pulmonary fibrosis [32–34]. The roles of HS in wound healing seem to be complicated and controversial. However, so far, no work has investigated the role of N-sulfated GAG on fibrosis.

In this study, we aim to investigate the effect of HS sulfation pattern alteration in mouse ADSCs by NDST1 overexpression. Although viral-based gene delivery is more efficient than nonviral-based gene delivery, there remain several concerns such as safety, immunogenic reactions, and tumorigenesis [35–37]. In this study, first, we evaluated and optimized the nonviral plasmid delivery efficiency into mouse ADSCs. Subsequently, we examined the effects of NDST1 overexpression in multiple aspects such as stemness, differentiation potency, inflammation response, and fibrotic response. Our study demonstrated that NDST1 overexpression suppressed osteogenic differentiation. In addition, we also showed that NDST1 overexpression attenuated a fibrotic response by suppressing collagen type I and alpha-smooth muscle production. This information facilitates the potential application of genetically modified ADSCs to prevent fibrosis.

Materials and Methods

Isolation and culture of mouse ADSCs

Inguinal adipose tissues of 14 weeks old C57BL/6J mice were harvested in accordance with the experimental guidelines and regulations approved by the University of Connecticut Health Center Institutional Animal Care and Use Committee (IACUC)–approved protocol (TE-101876-0821). In brief, adipose tissues were washed with Hank's Balanced Salt Solution (HBSS) and mechanically chopped before digestion with collagenase I (1,000 U/mL; Gibco) for 30 min at 37°C with intermittent shaking. The digested tissues were filtered through a 70-μm cell strainer (Thermo Fisher Scientific) and centrifuged at 800 *g* for 5 min. The cell pellets were incubated for 2 min in a red blood cell lysis buffer (Sigma Aldrich), and centrifuged again.

The final cell pellet was resuspended and placed in growth medium, which included DMEM/F12 basal medium, 10% fetal bovine serum, and 1% penicillin/streptomycin (Gibco) at 37°C and 5% CO_2 in a cell incubator. The cells were observed daily under an inverted phase-contrast microscope and were passaged after the cells reached 80%–90% confluency. The culture media was changed every 3 days. Three passaged mouse ADSCs were used in this study.

Flow cytometry

ADSCs were characterized by flow cytometry (ZE5 cell Analyzer 10; BioRad). Three passaged ADSCs (5×10^5 cells per sample) were collected and stained with fluorescein isothiocyanate (FITC)-conjugated rat anti-mouse CD90.2, CD11b, CD45, and CD31 (BD BioSciences) and phycoerythrin (PE)-conjugated rat anti-mouse CD29 (BD BioSciences), at a concentration of 2 μg/mL at 4°C for 30 min. To evaluate the transfection efficiency, transfected cells were collected and analyzed by flow cytometry for green fluorescent protein (GFP) expression. FlowJo software (Treestar, Inc.) was used for data visualization.

Plasmid constructs

Human NDST1 driven by a cytomegalovirus (CMV) promoter was synthesized in pcDNA 3.1+ plasmid (Genscript Company). Human and mice NDST1 share a very similar sequence where the overall amino acid identity is 98% (Supplementary Fig. S1). The plasmid pmaxGFP that encodes the enhanced GFP under CMV promoter (Lonza) was used to assess nucleofection efficiency and as a control for transfected cells.

Nucleofection of ADSCs

Six $\times 10^5$ mouse ADSCs and 2 μg of plasmid constructs were resuspended in 100 μL of nucleofection buffer from a human mesenchymal stem cell nucleofector kit (Lonza). Nucleofection was performed with an Amaxa nucleofector device (Lonza) using the following programs: X-001 (mouse T cells), C-017 (human MSCs, high viability), U-023 (human MSCs, high efficiency), A-023 (human stem cells), A-030 (mouse ESCs), and A-033 (mouse neural stem cells). After nucleofection, 500 μL of complete medium was added to the nucleofection cuvette, and cells were transferred into cell culture plates.

Cell viability measurement

Viable cells were counted following Trypan blue staining by using the Countess II Automated Cell Counter (Invitrogen). Cell viability was also assessed by CellTiter 96® AQueous One Solution Cell Proliferation Assay kit (MTS) (Promega) according to the manufacturer's instruction. In brief, cells were washed with phosphate-buffered saline (PBS), then an MTS reagent in a ratio of 5:1 (media: MTS) was added to each well. The plates were incubated for 2 h at 37°C. The absorbance of the resulting solution was read at 490 nm using a microplate reader.

Cell attachment measurement

Cells were fixed with 4% paraformaldehyde for 30 min. Cells were stained with crystal violet reagent (Sigma Aldrich) for 30 min, then rinsed with PBS until the solution became clear. After qualitative analysis by microscopy, the stain was eluted with 100% methanol and analyzed at 570 nm absorbance.

Colony-forming unit–fibroblast assay

Three thousand transfected ADSCs were cultured in 100 mm^2 dishes for 14 days. Cells were fixed with ice-cold methanol for 10 min, then incubated in 0.5% (w/v) crystal violet dissolved in 25% methanol for 10 min, followed by subsequent washing with tap water until the crystal violet stain was washed off and the culture dish was clear. The numbers of visible colonies formed on each dish were counted.

GAG sulfation analysis

Cells were grown in 12-well plates for 48 h after nucleofection and then incubated for 1 h at 37°C with 1 U/mL of Chondroitinase ABC (Sigma Aldrich) in PBS and 0.01% bovine serum albumin (BSA). The cells were digested by 3 U/mL of papain solution (Sigma Aldrich) for 3 h at 60°C. The level of GAG sulfation was quantified by the dimethylmethylene blue assay (Blyscan Assay Kit; Biocolor) according to the manufacturer's instruction.

DNA quantification

DNA was isolated and quantified using the Quant-iT PicoGreen dsDNA assay kit (Invitrogen) following the manufacturer's instructions. In brief, cell lysates were collected and mixed with the Quant-iT PicoGreen reagent, measured via spectrophotometry at 535 nm with excitation at 485 nm, and DNA content was quantified using a standard curve.

Western blotting

The cells were collected and lysed in CellLytic M (Sigma Aldrich) with protease inhibitor (Thermo Fisher Scientific) to obtain the total protein. The protein concentration was determined by the BCA protein assay kit (Thermo Fisher Scientific). Equal amounts of protein (10 μg) were separated by 10% SDS-PAGE and transferred onto a 0.2 mm Nitrocellulose Membrane. Then, the membranes were probed with an anti- beta-actin antibody (1:1,000; Abcam) or anti-NDST1 antibody (1:500; MyBioSource) diluted in 5% milk at 4°C overnight, followed by incubation with HRP-conjugated secondary antibodies (1:3,000; BioRad) at room temperature for 30 min. The SuperSignal™ West Pico PLUS Chemiluminescent Substrate (Thermo Fisher Scientific) was used for detection, and CL-XPosure Film (Thermo Fisher Scientific) was used for exposure of the membranes.

Differentiation potential of mouse ADSCs

For osteogenic induction, transfected mouse ADSCs were seeded in 24 well plates at 5.0×10^4 cells/well. After 24 h of culture, the media was replaced with StemPro osteogenic differentiation medium (Gibco) for 21 additional days. The medium was replaced every 3 days. Cells were fixed with 4% paraformaldehyde for 20 min at room temperature and stained with 0.2% Alizarin red S solution for 20 min at room temperature. After qualitative analysis by microscopy, the stain was eluted by 10% cetylpyridinium chloride for 15 min and analyzed at 450 nm absorbance.

For adipogenic induction, transfected mouse ADSCs were seeded in 24-well plates at 7.5×10^4 cells/well. After 24 h of culture, the medium was replaced with StemPro adipogenic differentiation medium (Gibco) for 14 additional days. The medium was replaced every 3 days. Cells were fixed with 4% paraformaldehyde for 20 min at room temperature and stained with Oil Red O solution for 20 min at room temperature. After qualitative analysis by microscopy, the stain was eluted by 100% isopropanol for 15 min and analyzed at 510 nm absorbance.

For chondrogenic induction, 2.0×10^5 transfected mouse ADSCs were pelleted in a 15-mL polypropylene tube and incubated with StemPro chondrogenic differentiation medium (Gibco) for 21 additional days. The medium was replaced every 3 days. GAG amount was quantified by the Blyscan Assay Kit as described above. For the histological section, cell pellets were fixed with 4% paraformaldehyde for 20 min at room temperature, embedded in paraffin, cut into 10 μm sections, and stained with 1% alcian blue (pH 1.0)/0.1% nuclear fast red.

Quantitative Real-Time PCR

Total RNA was extracted via standard protocols using commercial kits (RNeasy Mini Kit; Qiagen). Total RNA was reverse transcribed to cDNA by using RNA to cDNA EcoDry Premix (Clontech). Taqman predesigned primers (Thermo Fisher Scientific) (Supplementary Table S1) were used for quantitative real-time PCR (qRT-PCR), and the signal was detected by the CFX Connect Real-Time System (Bio-Rad). The threshold cycle values of target genes were standardized against GAPDH expression and normalized to the expression in the control culture. The fold change in expression was calculated using the ΔΔCq comparative threshold cycle method. Statistical analysis was performed for ΔΔCq values. All qRT-PCRs were run in quadruplicate.

Telomere length

Telomere length was evaluated by real-time PCR with the Relative Mouse Telomere Length Quantification qPCR Assay Kit (ScienCell Research Laboratories) following the manufacturer's protocol. Genomic DNAs extracted from transfected and untransfected cells were served as templates (2 ng/μL). Telomere-specific primers were used, and the signal was detected by the CFX Connect Real-Time System. The fold change in expression was calculated using the ΔΔCq comparative threshold cycle method normalized to the expression in the untransfected cells.

Cytokine array with tumor necrosis factor-α treatment

Transfected cells were seeded in 12-well plates. After 24 h, a fresh growth medium with recombinant human tumor necrosis factor-alpha (TNF-α) (10 ng/mL; R&D Systems) was added, and cells were cultured further for 24 h. Cell lysates were collected as described above and 150 μg of lysates were

used to detect growth factor/cytokines via mouse XL Cytokine Array Kit (R&D Systems) according to the manufacturer's protocol. Semiquantitative analysis based on the integrated density was performed by the ImageJ software.

TGF-β1 treatment

Transfected cells were seeded in 96-well plates and cultured overnight to over 90% confluency. Fresh growth medium with recombinant human transforming growth factor-beta1 (TGF-β1) (10 ng/mL; R&D systems) was added and cells were cultured for 24 h to induce a fibrogenic response. Cells were rinsed with PBS, fixed with 4% paraformaldehyde in PBS for 20 min at room temperature, and stained with Picrosirius red (0.1%) for 1 h.

Immunocytochemistry

TGF-β1-treated cells were rinsed with PBS, fixed with 4% paraformaldehyde in PBS for 20 min at room temperature, and permeabilized with 0.1% Triton × 100 for 10 min at room temperature. Next, cells were blocked with 1% BSA and incubated with anti-alpha-smooth muscle actin antibody (α-SMA) (1:25; Novus Biologicals) overnight at 4°C. Thereafter, cells were rinsed thrice with PBS and incubated with Goat Anti-Rabbit IgG H&L (Alexa Fluor® 594; Thermo Fisher Scientific) for 2 h at room temperature in the dark. DAPI (Invitrogen) was used as nuclear staining. All stained samples were examined under a Leica DMi8 inverted microscope (Leica Microsystems).

Statistical analysis

GraphPad Prism 7 (GraphPad Software) was used for statistical analysis and graph design. Results are expressed as the mean values ± standard deviation. Comparisons between two groups were performed with the unpaired Student's *t*-test. Differences were considered significant if the *P*-value was <0.05. Statistical significance was shown with $*P<0.05$, $**P<0.01$, $***P<0.001$, and $****P<0.0001$.

Results

Nucleofection optimization for mouse ADSCs

To confirm the success of mouse ADSCs isolation, the expressions of mesenchymal stem cell specific cell surface antigens were evaluated by flow cytometry. Mouse ADSCs at passage 3 were found to be positive for CD90.2 and CD29, and negative for CD11b, CD45, and CD31 (Supplementary Fig. S2A). Isolated mouse ADSCs have the capability of trilineage differentiation (Supplementary Fig. S2B–G). To examine the efficiency of nucleofection conditions for mouse ADSCs, different preset programs of nucleofection were tested and compared to the transfection efficiency and cell viability. Transfection efficiency was evaluated by GFP expression. The following programs were tested: X-001 (mouse T cells), C-017 (human MSCs, high viability), U-023 (human MSCs, high efficiency), A-023 (human stem cells), A-030 (mouse ESCs), and A-033 (mouse neural stem cells).

Although all programs could successfully induce GFP expression, the U-023 and A-033 program showed a higher number and brighter intensity of GFP-positive cells (Fig. 1A). When using the U-023 and A-033 programs, the expression of GFP in mouse ADSCs was ~50% (Fig. 1B, C). Cell viability was evaluated by counting live cell numbers and MTS assay. Although both programs confirmed that lower transfection efficiency facilitated higher cell viability (Fig. 1D, E), the U-023 program showed lower cell viability than the A-033 program.

Therefore, based on the comparison of transfection efficiency and cell viability, the A-033 program was chosen for the following experiment. By 14 days post-transfection, the number of GFP-positive cells were found to be very low in number and intensity (Fig. 1F, G). These transient GFP expression levels gradually decreased with incubation time and 16.5% ± 5.1% of cells ($n=3$) were positive for GFP at day 14 (Fig. 1H).

Gene delivery of NDST1 alters the sulfation pattern of HS

Six × 10^5 ADSCs were transfected with 2 μg of pmaxGFP (+GFP) or human NDST1 (+NDST1) according to the nucleofection protocol, using the A-033 program. NDST1 overexpression was confirmed by western blotting (Fig. 2A). The endogenous *NDST1* expression was evaluated by qRT-PCR. The result showed that NDST1 protein overexpression did not affect endogenous mouse NDST1 expression (Fig. 2B). To evaluate the effect of NDST1 on HS sulfation pattern, transfected cells were treated with chondroitinase to digest the chondroitin sulfate, followed by a collection of total GAGs. As expected, NDST1 overexpression increased the ratio of N-sulfation in the total GAGs (+GFP: 37.6% ± 6.6%, +NDST1: 50.0% ± 5.4%, Fig. 2C). Although there was no obvious morphological change after the transfection, we did observe lower cell attachment of NDST1-overexpressing cells compared to the GFP-expressing control (Fig. 2D–F).

Stemness and differentiation potency of NDST1-overexpressing cells

To determine whether transfected ADSCs can maintain their stem cell phenotype, mRNA levels of stem cell marker genes were evaluated by qRT-PCR. Pluripotent stem cell marker genes such as *Sox2* and *Rex1* showed the trends of increased expression in NDST1-overexpressing ADSCs, although the difference was not significant (Fig. 3A–C). Of note, the expression of *Oct-4* was below the detection limit at passage 3 of culture (data not shown). Similarly, NDST1 overexpression did not affect the number of colonies in colony-forming unit–fibroblast (Fig. 3D–F) nor the telomere length (Fig. 3G). Next, transfected mouse ADSCs were incubated under osteogenic, adipogenic, and chondrogenic medium conditions to evaluate the ability of multilineage differentiation. Osteogenic differentiation was assessed after 21 days in the osteogenic medium by Alizarin red staining. Notably, Alizarin red S stained-cells in the NDST1-overexpressing group were decreased compared to control (Fig. 3H–J).

Adipogenic differentiation was assessed after 14 days in the adipogenic medium by Oil Red O staining. There was no significant difference between controls and NDST1-overexpressing ADSCs. Thus, the NDST1 overexpression did not hinder the ability of ADSCs to differentiate into adipocytes (Fig. 3K–M). Likewise, the chondrogenic cultures were stained for GAG production after culture for

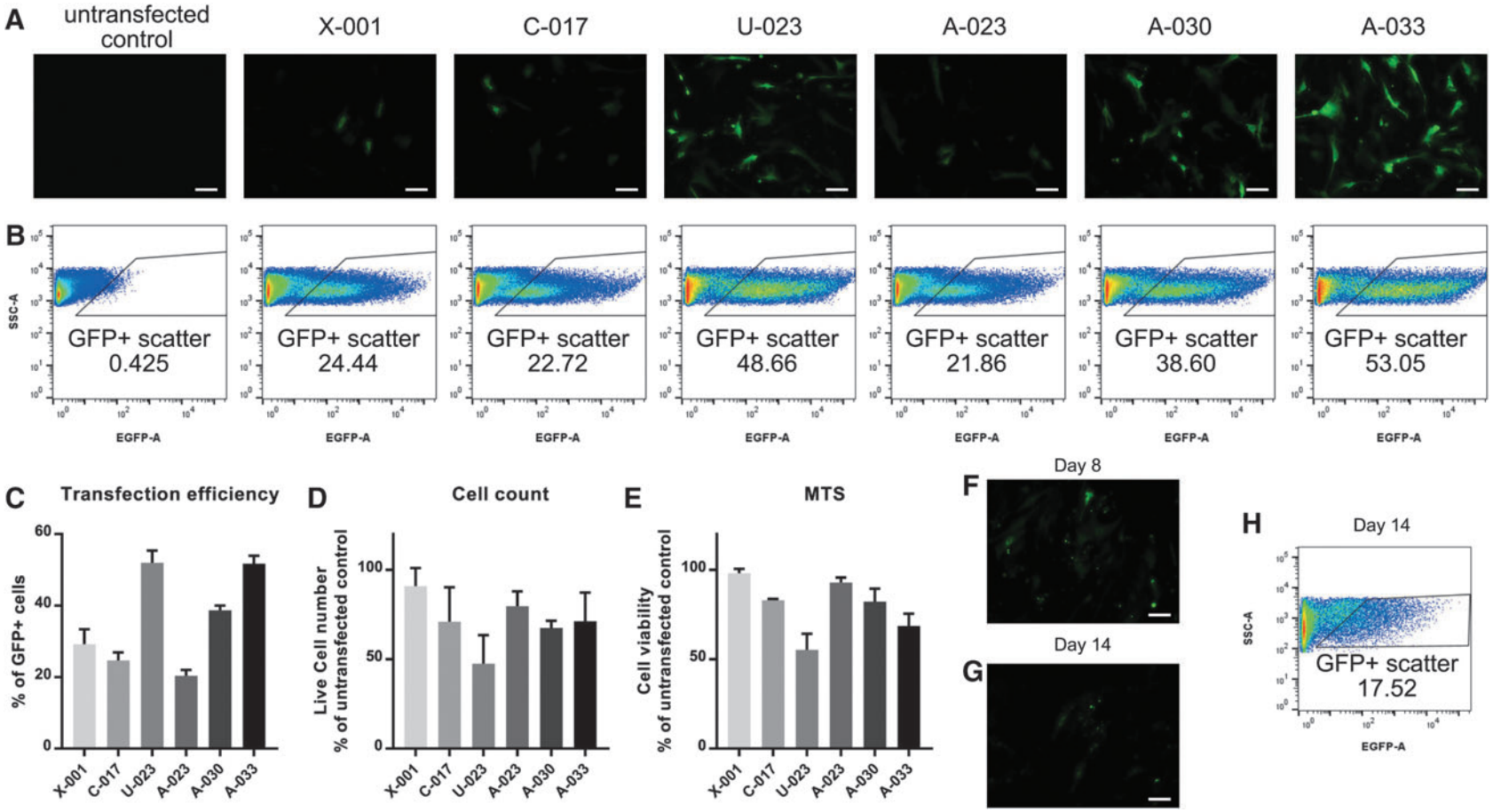

FIG. 1. Transfection efficiency and cell viability of mouse ADSCs. **(A)** Representative fluorescence images of transfected mouse ADSCs at 48 h after transfection. Mouse ADSCs were transfected with pmaxGFP construct using different nucleofection programs. **(B)** Representative flow cytometry analysis of transfected mouse ADSCs at 48 h after transfection. **(C)** Transfection efficiency for GFP expression of ADSCs. Data are expressed as a percentage of GFP-expressing cells determined by flow cytometry analysis ($n = 3$). **(D)** Cell viability calculated as a ratio of live cells to untransfected control. **(E)** MTS assay of transfected ADSCs normalized to untransfected control. **(F, G)** Representative fluorescence images of transfected mouse ADSCs at **(F)** 8 days and **(G)** 14 days after nucleofection (A-033). **(H)** Flow cytometry analysis of transfected mouse ADSCs at 14 days after transfection (A-033). Scale bar: 100 μm. ADSC, adipose-derived stem cell; GFP, green fluorescent protein.

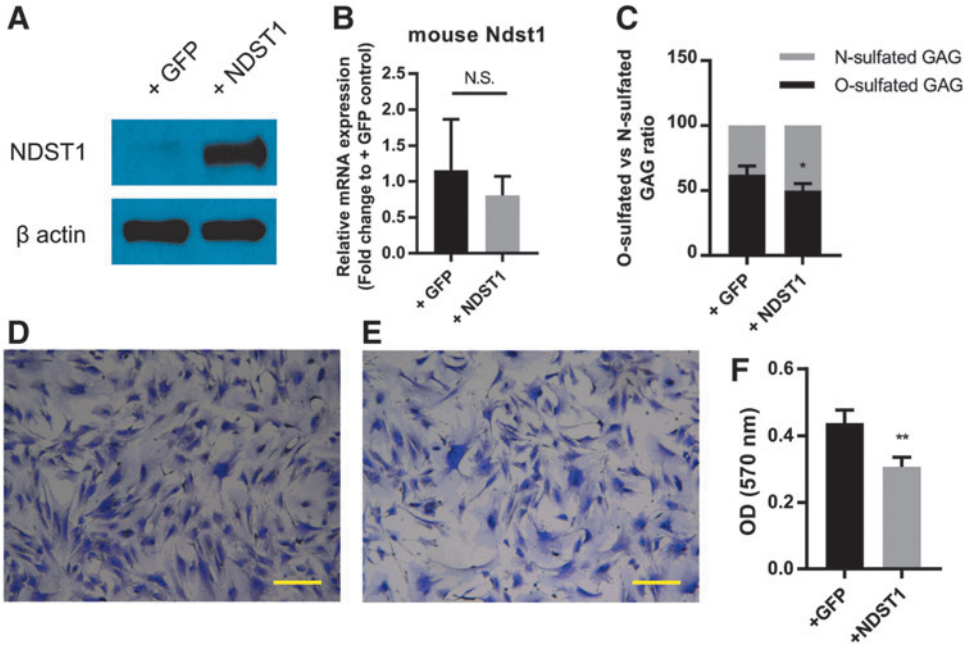

FIG. 2. Transfected ADSCs alter heparan sulfate composition. **(A)** Western blotting analysis for human NDST1 in transfected ADSCs. **(B)** qRT-PCR analysis for the mRNA levels of endogenous *NDST1* in transfected ADSCs. **(C)** The ratio of N-sulfated and O-sulfated GAG in transfected ADSCs. **(D, E)** Representative crystal violet staining images of **(D)** GFP- and **(E)** NDST1-overexpressing ADSCs. **(F)** Quantification of the attached cells was performed using the eluted crystal violet stain via measuring absorbance at 570 nm. N.S. no statistically significant, $*P < 0.05$, and $**P < 0.01$. Scale bar: 250 μm. qRT-PCR, quantitative real-time PCR; GAG, glycosaminoglycan.

21 days in the chondrogenic medium. The staining level and quantified total GAG amount of NDST1-overexpressed cultures were comparable to those of the control cultures (Fig. 3N–P).

Inflammatory response of NDST1-overexpressing cells

Since ADSCs are known for possessing anti-inflammatory effects via macrophage M1 to M2 transition [8], macrophage-related inflammatory gene expression was evaluated by qRT-PCR. The expression of chemokines that attract monocytes (*Csf1*) and macrophages (*Ccl2*) did not show statistically significant changes (Fig. 4A, B). The expression of proinflammatory gene (*Nos2*), proinflammatory cytokines (*TNF-α* and *IL-6*), and anti-inflammatory cytokines (*IL-10*) did not show statistically significant changes (Fig. 4C–F).

Next, we investigated the effect of NDST1 overexpression in the priming of ADSCs with the proinflammatory cytokine stimulation. The transfected ADSCs were stimulated with TNF α supplementation (10 ng/mL) for 24 h, then a membrane-based antibody array was used to determine the alteration of cytokine and chemokine production. The increased production of several chemokines that attract neutrophils and macrophages (CCL2, CXCL1, and CXCL2) were observed (Fig. 4G, H). The upregulation of gene expression was also confirmed by qRT-PCR (Fig. 4I–K). On the contrary, the trends of reduction for pro-/anti-inflammatory cytokines (TNF-α, IL-6, and IL-1ra) were observed (Fig. 4G, H). However, gene expression studies did not show any statistically significant differences between controls and NDST1-overexpressing ADSCs, including endogenous expression of TNF-α (Fig. 4L–N).

NDST1 overexpression attenuates fibrotic response

The subsequent studies investigated the regulation of fibrotic or anti-fibrotic gene expression in transfected ADSCs. NDST1 overexpression did not affect mRNA levels of *Tgfb1* and *Ctgf*, which are the major signaling molecules of fibrotic induction (Fig. 5A, B). Further, the expression of *Bgn*, one of the fibrotic marker genes, was not affected by NDST1 overexpression (Fig. 5C). However, the other fibrotic marker genes such as *Col1a1* and *Acta2* (*α-SMA*) were significantly downregulated in NDST1-overexpressing ADSCs (Fig. 5D, E). In contrast, antifibrotic gene expression (*Has2* and *Dcn*) showed upregulation in NDST1-overexpressing ADSCs (Fig. 5F, G). TGF-β1 (10 ng/mL) was used to induce a fibrotic response on transfected ADSCs.

After 24 h of treatment with TGF-β1, fibrotic ECM formation was visualized by Picrosirius red staining, indicating suppressed collagen synthesis in NDST1-overexpressing ADSCs (Fig. 5H). It is known that TGF-β1 treatment also disrupts the cell monolayer and induces cell migration to form nodules [38]. The production of α-SMA was found at the cell aggregates in the control group (Fig. 5I, yellow arrowheads), whereas it was dispersed in NDST1 overexpressing ADSCs (Fig. 5J).

Discussion

ADSCs are a widely used cell type in regenerative medicine due to their therapeutic potential. ADSCs are also used for cell-based gene therapy by overexpressing the desired factors [2]. Besides a safe, effective, and long-term gene delivery method, the survival of the cells after transplantation needs to be assessed for successful gene therapy. Most studies have been performed using viral vectors, which remains associated with safety concerns [37]. Alternatively, transfection of primary stem cells using nonviral methods such as classic calcium phosphate precipitation, cationic polymer, and standard electroporation result in reduced transfection efficiency [39]. Nucleofection is an electroporation-based method that enables DNA to directly enter the nucleus of a cell [40].

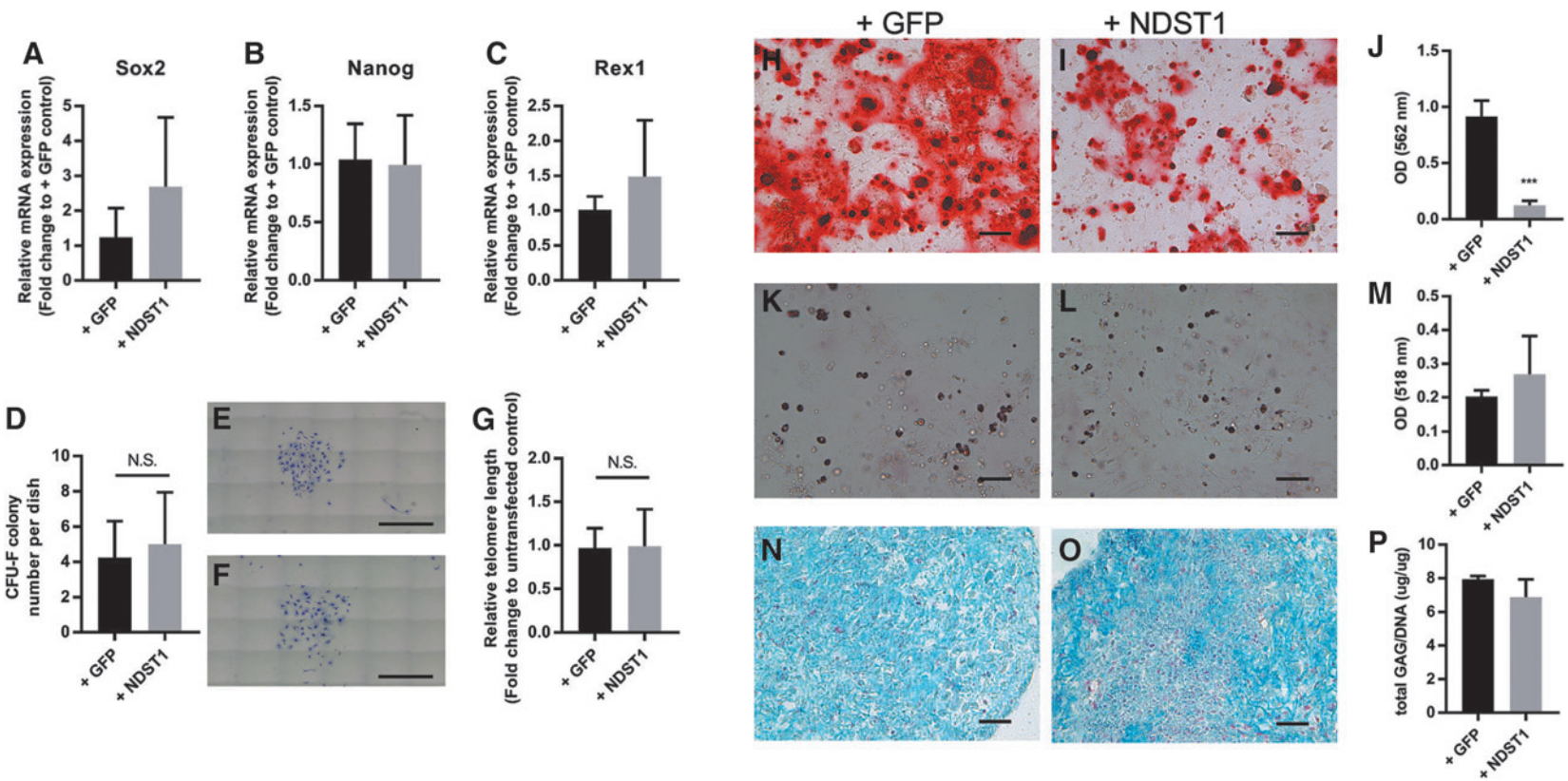

FIG. 3. Stemness and differentiation potential of transfected cells. **(A–C)** qRT-PCR analysis for the mRNA levels of **(A)** *Sox2*, **(B)** *Nanog*, and **(C)** *Rex1* in transfected ADSCs at 48 h after transfection. **(D)** CFU-F colonies from transfected ADSCs were counted after culture for 14 days. **(E, F)** Representative images of crystal violet staining of CFU-F assay for **(E)** GFP- and **(F)** NDST1-overexpressed ADSCs 14 days postseeding. **(G)** The relative telomere length normalized to untransfected control. **(H, I)** Osteogenic differentiation was confirmed by Alizarin red S staining after a 21-day culture of **(H)** GFP- and **(I)** NDST1-overexpressed ADSCs. **(J)** Quantification of the stained calcium deposit was performed using the eluted Alizarin red S stain via measuring absorbance at 450 nm. **(K, L)** Adipogenic differentiation was confirmed by Oil Red O staining after a 14-day culture of **(K)** GFP- and **(L)** NDST1-overexpressed ADSCs. **(M)** Quantification of the stained lipid droplets was performed using the eluted Oil red O stain via measuring absorbance at 510 nm. **(N, O)** Chondrogenic differentiation was confirmed by alcian blue/nuclear fast red staining of cell pellets section after a 21-day culture of **(N)** GFP- and **(O)** NDST1-overexpressed ADSCs. **(P)** Quantification of total GAG amount was measured by Blyscan Assay Kit normalized by DNA content. N.S. no statistically significant and $***P < 0.001$. Scale bar: 2 mm **(E, F)**; 100 μm **(H, I, K, L)**; 50 μm **(N, O)**. CFU-F, colony-forming unit–fibroblast.

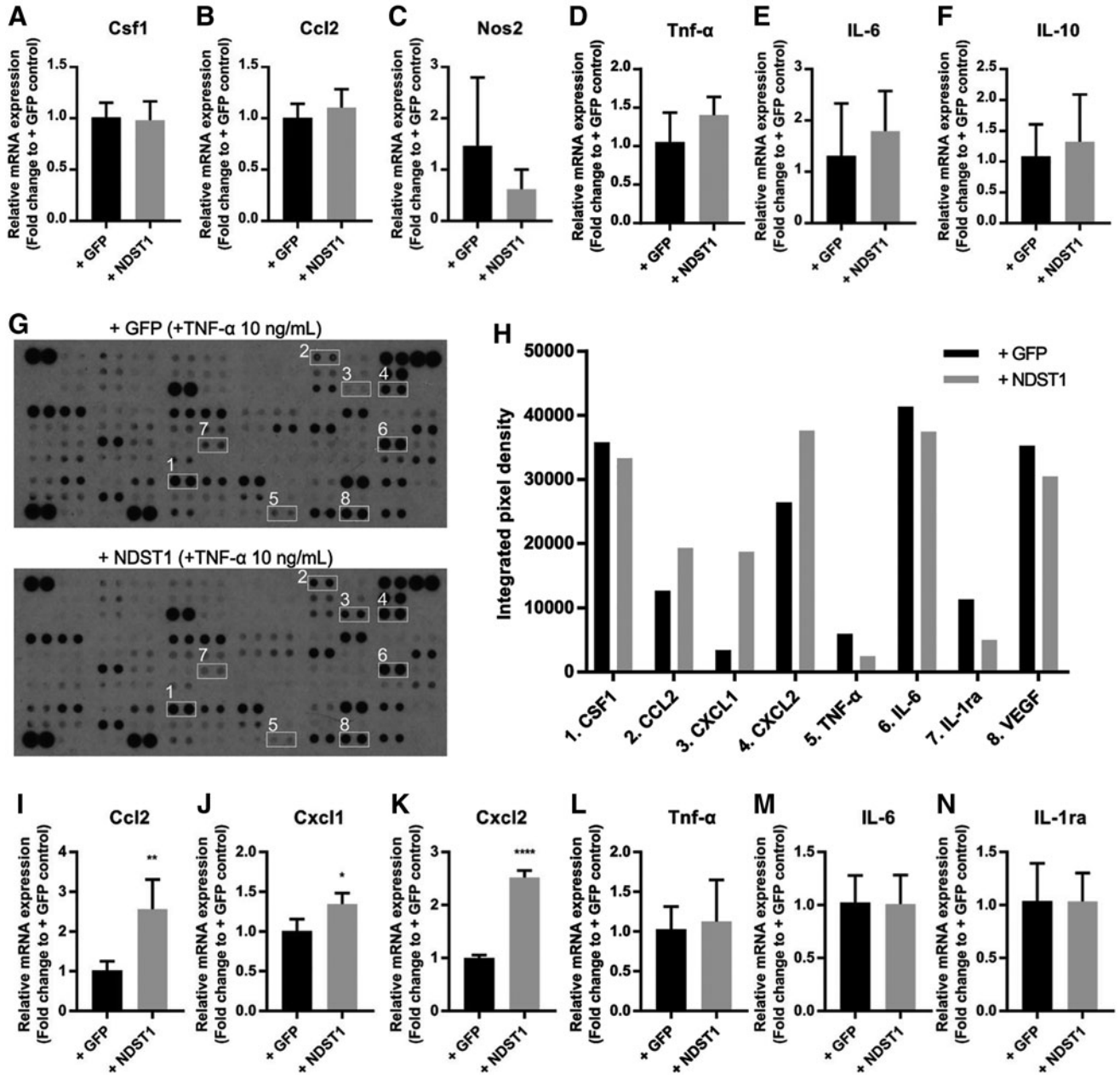

FIG. 4. Inflammatory gene expressions of transfected ADSCs. qRT-PCR analysis for the mRNA levels of **(A)** *Csf1*, **(B)** *Ccl2*, **(C)** *Nos2*, **(D)** *TNF-α*, **(E)** *IL-6*, and **(F)** *IL-10* in transfected ADSCs at 48 h after transfection. **(G)** Representative images of array membranes. The numbered spots were used for semiquantitative analysis. **(H)** Semiquantitative analysis showing integrated pixel density measurements of the data shown in **(G)**. qRT-PCR analysis for the mRNA levels of **(I)** *Ccl2*, **(J)** *Cxcl1*, **(K)** *Cxcl2*, **(L)** *TNF-α*, **(M)** *IL-6*, and **(N)** *IL-1ra* in transfected ADSCs at 24 h after TNF-α treatment (48 h after transfection). $*P < 0.05$, $**P < 0.01$, and $****P < 0.001$. TNF, tumor necrosis factor.

Several studies reported transplantation of mesenchymal stem cells with beneficial genes induced by nucleofection in vivo, resulting in expected outcomes [41,42]. Consistent with these studies, our results indicated a trade-off between transfection efficiency and cell viability (Fig. 1C–E). Transfection effects on gene expression are also expected to fade within 2 weeks (Fig. 1F–H).

HS chains are ubiquitously present at the cell surface of ESCs and are known to play a crucial role in the maintenance of pluripotency [43]. HS is also required for lineage commitment of ESCs and remodeling their sulfation pattern during differentiation. Lack of NDST1 in mouse ESCs cannot differentiate in response to FGF due to reduced sulfation [26]. In addition, exogenous HS supplementation enhances osteogenesis through the FGF2-FGFR1 signaling pathway [18]. In the present study, we described the effect of NDST1 overexpression on stemness and differentiation potency of mouse ADSCs.

Increased N-sulfated GAG content resulted in significant suppression of osteogenic differentiation (Fig. 2D–F). A

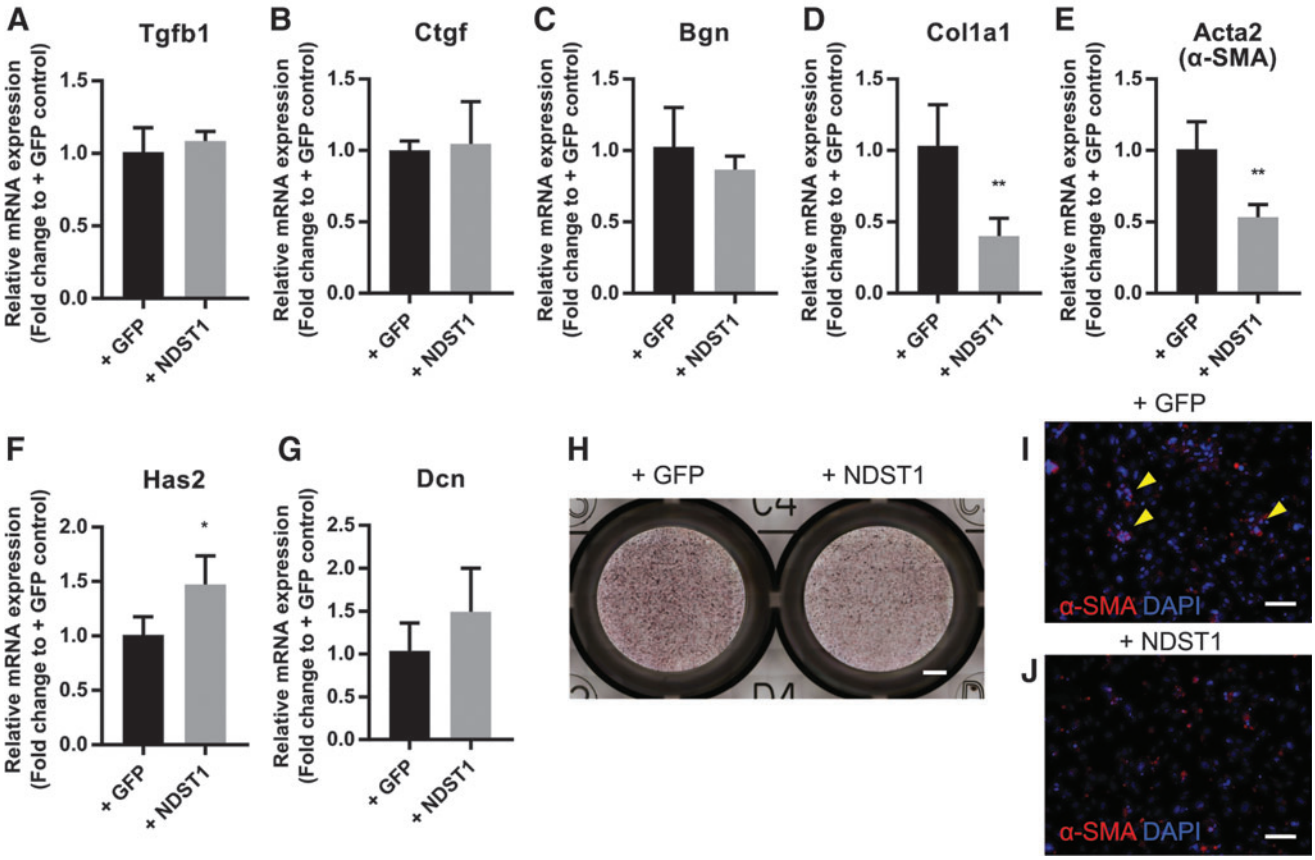

FIG. 5. Transfected ADSCs suppress fibrotic response. **(A–G)** qRT-PCR analysis for the mRNA levels of **(A)** *Tgfb1*, **(B)** *Ctgf*, **(C)** *Bgn*, **(D)** *Col1a1*, **(E)** *Acta2* (*α-SMA*), **(F)** *Has2*, and **(G)** *Dcn* in transfected ADSCs at 48 h after transfection. **(H)** Representative Picrosirius red staining images of transfected ADSCs stimulated for 24 h with TGF-b1. **(I, J)** Representative fluorescent images of **(I)** GFP- and **(J)** NDST1-overexpressed ADSCs stimulated for 24 h with TGF-b1 stained with α-SMA. *Yellow arrowheads* show cell aggregation that produces α-SMA. $^{*}P < 0.05$ and $^{**}P < 0.01$. Scale bar: 1 mm **(H)**; 100 μm **(I, J)**.

reduction in 6-O-sulfation impaired FGF2 signaling in aged neural stem cells has been reported [44]. Although 6-O-sulfation can occur independently of N-sulfation [45], increased N-sulfated GAG content might alter pro-osteogenic signal transduction. Moreover, we have shown type I collagen synthesis was significantly impeded in NDST1-overexpressing ADSCs (Fig. 5C). Type I collagen is the most abundant component of the bone ECM. The poor collagen content can lead to the abnormal bone formation, which can further result in osteogenesis imperfecta [46]. However, upregulation of NDST1 and Glypican-3 at the late stage of osteogenesis in the MC3T3 cell line has been reported [47]. Therefore, the combinatorial effect of sulfotransferases and HSPGs for temporal regulation of HS sulfation pattern still needs to be investigated.

HS is involved in the complex inflammation cascade by providing multiple binding sites for soluble mediators of the immune system. Therefore, biosynthetic enzymes possess an important role in the alteration of sulfation patterns in response to inflammatory stimuli [21]. For instance, depletion of NDST1 in macrophages produced more proinflammatory cytokines and chemokines in response to IFN-β stimulation [48]. However, little is known about the role of HS on the immunomodulatory effect of ADSCs. In the present study, we showed that NDST1 overexpression did not alter macrophage-related inflammatory gene expression compared to control (Fig. 4A–F). However, the external stimuli of inflammatory cytokines can boost soluble factors production of ADSCs and immune regulatory function [49]. Therefore, an extensive profile of soluble factors under cytokine stimulation was performed using a chemokine and cytokine array.

Although there was no notable alteration of cytokine productions, several chemokine productions (CCL2, CXCL1, and CXCL2) were upregulated (Fig. 4G–K). This result related to neutrophil attraction is consistent with the previous study that showed decreases in neutrophil infiltration in conditional NDST1-depleted mice [28]. Interestingly, these chemokines (CCL2, CXCL1, and CXCL2) were reported to possess binding affinity to distinct HS domains [50]. Furthermore, the combinatorial effect of CCL2 and IL-6 promoted M2 macrophage polarization [51]. We could not conclude the effect of NDST1 overexpression in immunomodulatory effect, however, further evaluation in the crosstalk with other immune cells such as neutrophils, macrophages, and T cells may provide functional roles of NDST1.

Based on our results, NDST1 plays a role in suppressing fibrotic response (Fig. 5). Interestingly, the expression of *Tgfb1* and its downstream mediator, *Ctgf*, was not affected by NDST1 overexpression (Fig. 5A, B). Although TGFb1 signaling has a central role in fibrosis, it is also required for

a successful regeneration process [52]. It should be noted that antifibrotic response independent of TGFb1 signaling may be considered as one of the beneficial effects for tissue regeneration. Increased HS production in damaged tissue, especially the upregulation of O-sulfation (3-, and 6-O-sulfation), has been reported in renal and pulmonary fibrosis [32–34]. Increased N-sulfated GAG by NDST1 overexpression might suppress the fibrotic response by impeding O-sulfated GAGs.

However, the mechanism of NDST1 in ECM production needs to be elucidated. The present study only showed the O- and N-sulfated GAG ratio. To fully understand the connection between complex oligosaccharides' structure and function, detailed glycomics and glycoproteomics analysis such as liquid chromatography, capillary electrophoresis, nuclear magnetic resonance, mass spectrometry, and microarrays should be used in the future to provide useful insights [53].

A limitation of the present study is that we could not achieve high efficiency of gene delivery protocol compared to viral-based gene delivery. Low transfection efficiency leads to a heterogeneous cell population, which may mask beneficial effects. Moreover, ADSCs have limited ability to proliferate in cultures and maintain their stemness [54–56], which makes it challenging to obtain a highly transfected cell population by long culture and selection. Therefore, it is important to develop high-efficiency and lengthy nonviral-based gene delivery systems into primary stem cells. Another direction is the use of immortalized ADSC as a stable cell source to obtain a conditioned medium that retains anti-inflammatory and antifibrosis effects [57,58]. Also, the comparison of N-sulfation levels among different mesenchymal stem cells will provide appropriate cell sources. These approaches will gain higher levels of N-sulfated GAG that might help to facilitate the development of new therapeutic strategies.

Conclusion

This study explored the optimum conditions of nonviral-based gene delivery in mouse ADSCs and described the fundamental effects of NDST1 overexpression on stem cell function. In this study, we showed that NDST1 overexpression suppressed osteogenic differentiation but did not affect adipogenic and chondrogenic differentiation. Furthermore, stemness and inflammatory gene expression were not affected by NDST1 overexpression. Finally, we demonstrated the potential of NDST1-overexpressing ADSCs in enhancing an antifibrotic response. Further studies are required to elucidate the mechanism of action of NDST1 on the regulation of HS sulfation and the subsequent effects on the regenerative process. Continued work on understanding the underlying mechanisms may also reveal new targets and treatments for the use of stem cell-based gene therapy.

Acknowledgments

The authors thank the histology core and flow cytometry core at UConn Health for their services. The authors also thank Dr. Peter F. Maye (Department of Reconstructive Sciences, UConn Health) for providing the nucleofector device. We gratefully acknowledge Ms. Michelle Slivinsky and Dr. Debolina Ghosh for proofreading the article.

Author Disclosure Statement

The authors have no conflicts of interest to declare.

Funding Information

This research was supported by funding from NIH DP1AR068147.

Supplementary Material

Supplementary Figure S1
Supplementary Figure S2
Supplementary Table S1

References

1. Tsuji W, J peter Rubin and KG Marra. (2014). Adipose-derived stem cells: implications in tissue regeneration. World J Stem Cells 6:312.
2. Zhang J, Y Liu, Y Chen, L Yuan, H Liu, J Wang, Q Liu and Y Zhang. (2020). Adipose-derived stem cells: current applications and future directions in the regeneration of multiple tissues. Stem Cells Int 2020:8810813.
3. Zhou Y, Y Yamamoto, Z Xiao and T Ochiya. (2019). The immunomodulatory functions of mesenchymal stromal/stem cells mediated via paracrine activity. J Clin Med 8: 1025.
4. Daneshmandi L, S Shah, T Jafari, M Bhattacharjee, D Momah, N Saveh-Shemshaki, KWH Lo and CT Laurencin. (2020). Emergence of the stem cell secretome in regenerative engineering. Trends Biotechnol 38:1373–1384.
5. Gao F, SM Chiu, DAL Motan, Z Zhang, L Chen, HL Ji, HF Tse, QL Fu and Q Lian. (2016). Mesenchymal stem cells and immunomodulation: current status and future prospects. Cell Death Dis 7:e2062.
6. Ceccarelli S, P Pontecorvi, E Anastasiadou, C Napoli and C Marchese. (2020). Immunomodulatory effect of adipose-derived stem cells: the cutting edge of clinical application. Front Cell Dev Biol 8:1–12.
7. Pilny E, R Smolarczyk, M Jarosz-Biej, A Hadyk, A Skorupa, M Ciszek, Ł Krakowczyk, N Kułach, D Gillner, et al. (2019). Human ADSC xenograft through IL-6 secretion activates M2 macrophages responsible for the repair of damaged muscle tissue. Stem Cell Res Ther 10:1–20.
8. Heo JS, Y Choi, HO Kim and C Matta. (2019). Adipose-derived mesenchymal stem cells promote M2 macrophage phenotype through exosomes. Stem Cells Int 2019: 7921760.
9. Costalonga EC, C Fanelli, MR Garnica and IL Noronha. (2020). Adipose-derived mesenchymal stem cells modulate fibrosis and inflammation in the peritoneal fibrosis model developed in uremic rats. Stem Cells Int 2020:3768718.
10. Kotani T, R Masutani, T Suzuka, K Oda, S Makino and M Ii. (2017). Anti-inflammatory and anti-fibrotic effects of intravenous adipose-derived stem cell transplantation in a mouse model of bleomycin-induced interstitial pneumonia. Sci Rep 7:1–10.
11. Yang CY, PY Chang, JY Chen, BS Wu, AH Yang and OKS Lee. (2021). Adipose-derived mesenchymal stem cells attenuate dialysis-induced peritoneal fibrosis by modulating macrophage polarization via interleukin-6. Stem Cell Res Ther 12:1–12.
12. Sarrazin S, WC Lamanna and JD Esko. (2011). Heparan sulfate proteoglycans. Cold Spring Harb Perspect Biol 3:1–33.

13. Bishop JR, M Schuksz and JD Esko. (2007). Heparan sulphate proteoglycans fine-tune mammalian physiology. Nature 446:1030–1037.
14. Lin X. (2004). Functions of heparan sulfate proteoglycans in cell signaling during development. Development 131: 6009–6021.
15. Papy-Garcia D and P Albanese. (2017). Heparan sulfate proteoglycans as key regulators of the mesenchymal niche of hematopoietic stem cells. Glycoconj J 34:377–391.
16. Ravikumar M, RAA Smith, V Nurcombe and SM Cool. (2020). Heparan sulfate proteoglycans: key mediators of stem cell function. Front Cell Dev Biol 8:1–23.
17. Jackson RA, V Nurcombe and SM Cool. (2006). Coordinated fibroblast growth factor and heparan sulfate regulation of osteogenesis. Gene 379:79–91.
18. Dombrowski C, SJ Song, P Chuan, X Lim, E Susanto, AA Sawyer, MA Woodruff, DW Hutmacher, V Nurcombe and SM Cool. (2009). Heparan sulfate mediates the proliferation and differentiation of rat mesenchymal stem cells. Stem Cells Dev 18:661–670.
19. Okolicsanyi RK, LE Oikari, C Yu, LR Griffiths and LM Haupt. (2018). Heparan sulfate proteoglycans as drivers of neural progenitors derived from human mesenchymal stem cells. Front Mol Neurosci 11:134.
20. Farrugia BL, MS Lord, J Melrose and JM Whitelock. (2018). The role of heparan sulfate in inflammation, and the development of biomimetics as anti-inflammatory strategies. J Histochem Cytochem 66:321–336.
21. Collins LE and L Troeberg. (2019). Heparan sulfate as a regulator of inflammation and immunity. J Leukoc Biol 105:81–92.
22. Phan AQ, J Lee, M Oei, C Flath, C Hwe, R Mariano, T Vu, C Shu, A Dinh, et al. (2015). Positional information in axolotl and mouse limb extracellular matrix is mediated via heparan sulfate and fibroblast growth factor during limb regeneration in the axolotl (*Ambystoma mexicanum*). Regeneration 2:182–201.
23. Otsuka T, AQ Phan, CT Laurencin, JD Esko, S V. Bryant and DM Gardiner. (2020). Identification of heparan-sulfate rich cells in the loose connective tissues of the axolotl (Ambystoma mexicanum) with the potential to mediate growth factor signaling during regeneration. Regen Eng Transl Med 6:7–17.
24. Bame KJ and JD Esko. (1989). Undersulfated heparan sulfate in a Chinese hamster ovary cell mutant defective in heparan sulfate N-sulfotransferase. J Biol Chem 264:8059–8065.
25. Pikas DS, I Eriksson and L Kjellén. (2000). Overexpression of different isoforms of glucosaminyl N-deacetylase/N-sulfotransferase results in distinct heparan sulfate N-sulfation patterns. Biochemistry 39:4552–4558.
26. Lanner F, KL Lee, M Sohl, K Holmborn, H Yang, J Wilbertz, L Poellinger, J Rossant and F Farnebo. (2010). Heparan sulfation-dependent fibroblast growth factor signaling maintains embryonic stem cells primed for differentiation in a heterogeneous state. Stem Cells 28:191–200.
27. Olczyk P, Ł Mencner and K Komosinska-Vassev. (2015). Diverse roles of heparan sulfate and heparin in wound repair. Biomed Res Int 2015:549417.
28. Wang L, M Fuster, P Sriramarao and JD Esko. (2005). Endothelial heparan sulfate deficiency impairs L-selectin- and chemokine-mediated neutrophil trafficking during inflammatory responses. Nat Immunol 6:902–910.
29. Zhou Z, J Wang, R Cao, H Morita, R Soininen, KM Chan, B Liu, Y Cao and K Tryggvason. (2004). Impaired angiogenesis, delayed wound healing and retarded tumor growth in Perlecan heparan sulfate-deficient mice. Cancer Res 64:4699–4702.
30. Echtermeyer F, M Streit, S Wilcox-Adelman, S Saoncella, F Denhez, M Detmar and PF Goetinck. (2001). Delayed wound repair and impaired angiogenesis in mice lacking syndecan-4. J Clin Invest 107:9–14.
31. Zcharia E, R Zilka, A Yaar, O Yacoby-Zeevi, A Zetser, S Metzger, R Sarid, A Naggi, B Casu, et al. (2005). Heparanase accelerates wound angiogenesis and wound healing in mouse and rat models. FASEB J 19:211–221.
32. Alhasan AA, J Spielhofer, M Kusche-Gullberg, JA Kirby and S Ali. (2014). Role of 6-O-sulfated heparan sulfate in chronic renal fibrosis. J Biol Chem 289:20295–20306.
33. Lu J, L Auduong, ES White and X Yue. (2014). Up-regulation of heparan sulfate 6-O-sulfation in idiopathic pulmonary fibrosis. Am J Respir Cell Mol Biol 50:106–114.
34. Ferreras L, A Moles, GR Situmorang, R El Masri, IL Wilson, K Cooke, E Thompson, M Kusche-Gullberg, RR Vivès, NS Sheerin and S Ali. (2019). Heparan sulfate in chronic kidney diseases: exploring the role of 3-O-sulfation. Biochim Biophys Acta Gen Subj 1863:839–848.
35. Yin H, RL Kanasty, AA Eltoukhy, AJ Vegas, JR Dorkin and DG Anderson. (2014). Non-viral vectors for gene-based therapy. Nat Rev Genet 15:541–555.
36. Patil S, YG Gao, X Lin, Y Li, K Dang, Y Tian, WJ Zhang, SF Jiang, A Qadir and AR Qian. (2019). The development of functional non-viral vectors for gene delivery. Int J Mol Sci 20:1–23.
37. Shayakhmetov DM, NC Di Paolo and KL Mossman. (2010). Recognition of virus infection and innate host responses to viral gene therapy vectors. Mol Ther 18:1422–1429.
38. Xu Q, JT Norman, S Shrivastav, J Lucio-Cazana and JB Kopp. (2007). In vitro models of TGF-β-induced fibrosis suitable for high-throughput screening of antifibrotic agents. Am J Physiol Ren Physiol 293:F631–F640.
39. Halim NSSA, KS Fakiruddin, SA Ali and BH Yahaya. (2014). A comparative study of non-viral gene delivery techniques to human adipose-derived mesenchymal stem cell. Int J Mol Sci 15:15044–15060.
40. Distler JHW, A Jüngel, M Kurowska-Stolarska, BA Michel, RE Gay, S Gay and O Distler. (2005). Nucleofection: a new, highly efficient transfection method for primary human keratinocytes. Exp Dermatol 14:315–320.
41. Mizrahi O, D Sheyn, W Tawackoli, I Kallai, A Oh, S Su, X Da, P Zarrini, G Cook-Wiens, D Gazit and Z Gazit. (2013). BMP-6 is more efficient in bone formation than BMP-2 when overexpressed in mesenchymal stem cells. Gene Ther 20:370–377.
42. Scheibe F, N Gladow, P Mergenthaler, AH Tucker, A Meisel, DJ Prockop and J Priller. (2012). Nonviral gene delivery of erythropoietin by mesenchymal stromal cells. Gene Ther 19:550–560.
43. Sasaki N, K Okishio, K Ui-Tei, K Saigo, A Kinoshita-Toyoda, H Toyoda, T Nishimura, Y Suda, M Hayasaka, K Hanaoka, S Hitoshi, K Ikenaka and S Nishihara. (2008). Heparan sulfate regulates self-renewal and pluripotency of embryonic stem cells. J Biol Chem 283:3594–3606.
44. Yamada T, A Kerever, Y Yoshimura, Y Suzuki, R Nonaka, K Higashi, T Toida, F Mercier and E Arikawa-Hirasawa. (2017). Heparan sulfate alterations in extracellular matrix structures and fibroblast growth factor-2 signaling impairment in the aged neurogenic niche. J Neurochem 142:534–544.

45. Holmborn K, J Ledin, E Smeds, I Eriksson, M Kusche-Gullberg and L Kjellén. (2004). Heparan sulfate synthesized by mouse embryonic stem cells deficient in NDST1 and NDST2 is 6-O-sulfated but contains no N-sulfate groups. J Biol Chem 279:42355–42358.
46. Tzaphlidou M. (2008). Bone architecture: collagen structure and calcium/phosphorus maps. J Biol Phys 34: 39–49.
47. Haupt LM, S Murali, KM Foong, N Teplyuk, FM Leong, GS Stein, AJ Van Wijnen, V Nurcombe and SM Cool. (2009). The heparan sulfate proteoglycan (HSPG) glypican-3 mediates commitment of MC3T3-E1 cells toward osteogenesis. J Cell Physiol 220:780–791.
48. Gordts PLSM, EM Foley, R Lawrence, R Sinha, C Lameda-Diaz, L Deng, R Nock, CK Glass, A Erbilgin, et al. (2014). Reducing macrophage proteoglycan sulfation increases atherosclerosis and obesity through enhanced type i interferon signaling. Cell Metab 20:813–826.
49. Boland L, AJ Burand, AJ Brown, D Boyt, VA Lira and JA Ankrum. (2018). IFN-γ and TNF-α Pre-licensing protects mesenchymal stromal cells from the pro-inflammatory effects of palmitate. Mol Ther 26:860–873.
50. Van Gemst JJ, M Kouwenberg, ALWMM Rops, TH Van Kuppevelt, JH Berden, TJ Rabelink, MA Loeven and J Van Der Vlag. (2018). Differential binding of chemokines CXCL1, CXCL2 and CCL2 to mouse glomerular endothelial cells reveals specificity for distinct heparan sulfate domains. PLoS One 13:1–15.
51. Roca H, ZS Varcos, S Sud, MJ Craig and KJ Pienta. (2009). CCL2 and interleukin-6 promote survival of human CD11b+ peripheral blood mononuclear cells and induce M2-type macrophage polarization. J Biol Chem 284: 34342–34354.
52. Otsuka T, HM Kan and CT Laurencin. (2021). Regenerative engineering approaches to scar-free skin regeneration. Regen Eng Transl Med [Epub ahead print]; DOI: 10.1007/s40883-021-00229-8.
53. Abrahams JL, G Taherzadeh, G Jarvas, A Guttman, Y Zhou and MP Campbell. (2020). Recent advances in glycoinformatic platforms for glycomics and glycoproteomics. Curr Opin Struct Biol 62:56–69.
54. Taha MF and V Hedayati. (2010). Isolation, identification and multipotential differentiation of mouse adipose tissue-derived stem cells. Tissue Cell 42:211–216.
55. Zhao Y, SD Waldman and LE Flynn. (2012). The effect of serial passaging on the proliferation and differentiation of bovine adipose-derived stem cells. Cells Tissues Organs 195:414–427.
56. Chen HT, MJ Lee, CH Chen, SC Chuang, LF Chang, ML Ho, SH Hung, YC Fu, YH Wang, et al. (2012). Proliferation and differentiation potential of human adipose-derived mesenchymal stem cells isolated from elderly patients with osteoporotic fractures. J Cell Mol Med 16:582–592.
57. Oki K, S Yoshihara, N Urushihata and M Ghazizadeh. (2021). Anti-fibrotic effect of adipose-derived mesenchymal stem cell conditioned medium in muscle fibrosis. Eur Rev Med Pharmacol Sci 25:4953–4963.
58. Kruger MJ, MM Conradie, M Conradie and M Van De Vyver. (2018). ADSC-conditioned media elicit an ex vivo anti-inflammatory macrophage response. J Mol Endocrinol 61:173–184.

Address correspondence to:
Cato T. Laurencin, MD, PhD
Connecticut Convergence Institute for Translation in Regenerative Engineering
University of Connecticut Health
Farmington, CT 06032-1941
USA

E-mail: laurencin@uchc.edu

Received for publication February 16, 2022
Accepted after revision August 1, 2022
Prepublished on Liebert Instant Online August 3, 2022